PLANT SCIENCES

Diversification of ranunculaceous petals in shape supports a generalized model for plant lateral organ morphogenesis and evolution

Jie Cheng[1,2]†, Xu Yao[1,2]†, Xukun Li[1,2,3]†, Liang Yue[1], Xiaoshan Duan[1], Boka Li[1,2,3], Xuehao Fu[1,2], Shuixian Li[1,2,3], Hongyan Shan[1,2], Xiaofeng Yin[1,2], Christopher Whitewoods[4], Enrico Coen[5], Hongzhi Kong[1,2,3]*

Peltate organs, such as the prey-capturing traps of carnivorous plants and nectary-bearing petals of ranunculaceous species, are widespread in nature and have intrigued and perplexed scientists for centuries. Shifts in the expression domains of adaxial/abaxial genes have been shown to control leaf peltation in some carnivorous plants, yet the mechanisms underlying the generation of other peltate organs remain unclear. Here, we show that formation of various peltate ranunculaceous petals was also caused by shifts in the expression domains of adaxial/abaxial genes, followed by differentiated regional growth sculpting the margins and/or other parts of the organs. By inducing parameters to specify the time, position, and degree of the shifts and growth, we further propose a generalized modeling system, through which various unifacial, bifacial, and peltate organs can be simulated. These results demonstrate the existence of a hierarchical morphospace system and pave the way to understand the mechanisms underlying plant organ diversification.

INTRODUCTION

Sterile lateral organs of plants, such as leaves, sepals, and petals, are generally flat or slightly curved planar structures with distinct adaxial and abaxial sides (i.e., bifacial). Many plants, however, produce highly specialized, nonplanar organs that either lack the adaxial or abaxial side (i.e., unifacial) or have a bifacial lamina and a unifacial stalk (e.g., peltate) (*1*). Peltate organs have been documented in many flowering plants and can be further classified into several subtypes (e.g., cup-shaped, tubular, and utricular), although the boundaries among them are not always distinct (*2*). It has been proposed that peltate organs are usually results of adaptation to animal visitors, good examples of which are the prey-capturing leaves or leaflets of carnivorous plants [e.g., *Utricularia gibba* (Lentibulariaceae), *Sarracenia purpurea* (Sarraceniaceae), and *Cephalotus follicularis* (Cephalotaceae)] and the nectary-bearing petals of some ranunculaceous species (e.g., *Nigella damascena*, *Helleborus thibetanus*, and *Dichocarpum fargesii*) (*3*–*5*). The mechanisms underlying the formation, origin, and diversification of the various subtypes of peltate organs, yet, remain largely unclear, although they have intrigued and perplexed scientists (including the most famous naturalist, Charles Darwin) for centuries (*1*, *6*).

Nevertheless, it has been suggested that to form a peltate organ, the formation of the so-called *Querzone* (i.e., the transverse zone resulted from the congenital fusion of the ectopic proximal margins) is usually the key (*1*). At the histological level, the outgrowth of the *Querzone* can be achieved through periclinal division of one or two groups of subepidermal cells in the primordia (*5*, *7*). At the molecular level, however, it may be caused by shifts in the expression domains of the antagonistically functioning adaxial and abaxial genes (*8*). Adaxial genes, such as homologs of class III homeodomain-leucine zipper (HD-ZIP III) transcription factors [i.e., *REVOLUTA* (*REV*), *PHABULOSA* (*PHB*), and *PHAVOLUTA* (*PHV*)], *ASYMMETRIC LEAVES 1/2* (*AS1/2*), and trans-acting small interfering RNAs (ta-siRNAs), are usually expressed in the upper side of a bifacial lateral organ and specify the adaxial identity; inactivation of them leads to the generation of abaxially needle-like or rod-/trumpet-shaped phenotypes (*9*–*12*). Abaxial genes, such as counterparts of *AUXIN RESPONSE FACTOR 3/4* (*ARF3/4*), *KANADIs* (*KANs*), *YABBYs* (*YABs*), and miRNA165/166, in contrast, are often expressed in the lower side of the organ and specify its abaxial identity; inactivation of them leads to the generation of adaxially radialized or cup-shaped forms (*13*–*17*). When the balance between the adaxial and abaxial functions was broken by shifting (rather than completely inactivating) the expression domains of key adaxial/abaxial genes, new balances would be reached, and thus, the organ would become peltate, as in the cases of *Tropaeolum majus* (Tropaeolaceae), *U. gibba*, and *S. purpurea*, whose leaves/leaflets are shield-shaped, utricular, and pitcher-shaped, respectively (*18*–*20*).

Notably, in most of the aforementioned cases, the conclusions were drawn not on the basis of detailed functional studies because, like the situations in many other nonmodel species, genetic or transgenic manipulations of the plants have been extremely difficult and/or very time-consuming. Rather, expression patterns of key candidate genes and computational modeling of corresponding developmental processes have been the key (*19*, *20*). By setting the parameters that reflect the activities of different morphogens and adjusting their values, computational simulation can not only recur the developmental processes of various plant lateral organs but also help predict the not-yet-found regulators of key

[1]State Key Laboratory of Systematic and Evolutionary Botany, CAS Center for Excellence in Molecular Plant Sciences, Institute of Botany, Chinese Academy of Sciences, Beijing 100093, China. [2]China National Botanical Garden, Beijing 100093, China. [3]University of Chinese Academy of Sciences, Beijing 100049, China. [4]Sainsbury Laboratory, University of Cambridge, Cambridge CB2 1LR, UK. [5]Department of Cell and Developmental Biology, John Innes Centre, Norwich Research Park, Colney Lane, Norwich NR4 7UH, UK.
*Corresponding author. Email: hzkong@ibcas.ac.cn
†These authors contributed equally to this work.

morphological changes, thereby guiding the functional studies on nonmodel species. The problem, however, is twofold. On the one hand, the available models were built almost all for leaves or leaflets; it is, therefore, unclear whether they also apply to other types of plant lateral organs (e.g., petals). On the other hand, because the existing models were built in a case-by-case manner, with different parameters being induced in different species, it is unclear whether diverse shapes can be generated in a single modeling system. To solve these problems, investigations on plant groups with abundant diversity in the basic shapes of the same or comparable organs are needed.

The buttercup family (Ranunculaceae) appears to be an excellent system for the study of the mechanisms underlying plant lateral organ development and evolution, for three reasons. First, in the family, while some species produce flat or spurred bifacial petals, many taxa bear peltate petals that exhibit a huge wealth of morphological diversity, being tubular, bilabiate, spoon-like, or goblet-shaped (Fig. 1, A to J, and fig. S1). Second, the developmental processes of many ranunculaceous petals have been studied extensively, based on which a few hypotheses have been proposed to explain the trajectories and possible mechanisms underlying their ontogeny and evolution (Fig. 1K) (*4*, *21*). Specifically, it has been proposed that while the formation of a *Querzone* is always a prerequisite for petal peltation, the final shape of the organ is determined by activities of other factors (such as differentiated rates of growth) (*22*). Third, some members of the family (e.g., *Aquilegia coerulea* and *N. damascena*) have been developed into model systems, to which virus-induced gene silencing (VIGS) and other functional approaches are applicable (*23*–*26*), so that the hypotheses proposed, if any, can be tested.

Here, by using petals of ranunculaceous species as a research system and conducting extensive morphological, three-dimensional (3D) imaging, expression, functional, and computational modeling studies, we attempt to understand the mechanisms underlying the formation and diversification of peltate structures and establish a generalized modeling system for the formation of diverse plant lateral organs.

RESULTS

Development of *N. damascena* petals and expression of key adaxial/abaxial genes

To understand how peltate petals were made through development, we first investigated the ontogeny of the *N. damascena* petals that each has a unifacial rod-like stalk and two reversely arranged bifacial lips (i.e., including a small laminar upper lip and a relatively large, doubly bended and terminally bifurcated lower lip) (Fig. 2, A and B). At the very early stage of development (i.e., stage 1), the primordium of the petal was dome-shaped, resembling those of bifacial petals in other species but differing slightly from those of leaves, bracts, or sepals, which are nearly crescent from inception (*27*). As the primordium grew up (i.e., stages 2 and 3), its distal half flattened, whereas the proximal half narrowed down, although the entire organs remained bifacial. Later (i.e., stages 4 and 5), due to the emergence of the *Querzone*, the upper lip appeared and the petal became bilabiate, with a stalk being formed at its base and a nectar chamber being formed between the upper and lower lips (Fig. 2, C to E). During the later stages of petal development (i.e., from stage 6 on), a sinus was formed on the developing lower lip (i.e., the dorsal lobe) and the entire organ enlarged while preserving other morphological features (Fig. 2E). Clearly, the formation of the *N. damascena* petal is a progressive process, with peltation of the primordium being the first step, followed by modifications of other parts.

To explore the mechanism underlying petal peltation in *N. damascena*, we first isolated homologs of the key adaxial and abaxial genes (fig. S2) and examined their expression patterns. We found that, at the early stages of petal development (stages 1 to 3), the adaxial genes *NidaPHX* (a homolog of *PHB/PHV*-related genes), *Nida HOMEOBOX GENE 8* (*NidaHB8*), and *NidaAS2* were expressed in the adaxial side of the primordia, whereas the abaxial gene *NidaYAB5* and miR166 were expressed in the abaxial side, suggestive of balanced expression (Fig. 2F and fig. S3). Then, slightly before the establishment of the *Querzone* at stage 4, the expression domains of *NidaPHX*, *NidaAS2*, and *NidaHB8* contracted to the distal part of the adaxial side of the elongated petal primordia, whereas those of miR166 and *NidaYAB5* (at stage 5) expanded from the abaxial side to the proximal part of the adaxial side of the primordia (Fig. 2F and fig. S3), suggestive of shifts in the expression domains of adaxial and abaxial genes. Thereafter (e.g., stage 6), the balance between the expression of abaxial and adaxial genes was restored in the growing upper and lower petal lips, respectively. Clearly, the formation of peltate petals is also tightly related to shifts in the expression domains of adaxial and abaxial genes.

Simulation of the *N. damascena* petals and functional tests of its reliability

To gain more insights into how the shifts in the expression domains of adaxial and abaxial genes have caused peltation of the petals, we conducted simulations in a previously proposed polarity-based modeling system (*28*). In this system, the growth of a 3D organ was specified by setting two orthogonal polarity fields (i.e., orthoplanar and proximodistal) and three growth rates (i.e., one parallel to the orthoplanar polarity field, K_{op}, one parallel to the proximodistal polarity field, K_{pd}, and one perpendicular to the former two, K_{per}) that determine the thickening, elongating, and widening of a planar structure, respectively. The orthoplanar polarity field was established by taking the gradient of a morphogen (POL) diffusing from the surface to the central core (CORE) and midplane (MIP) of the adaxial (AD) and abaxial (AB) domains of a hemispheric organ primordium, whereas the proximodistal polarity field was established by taking the gradient of another morphogen (POL2) diffusing from the base to the tip (Fig. 3A). For the set of growth rates, a total of five factors (BLA, STK, MID_DOR, MID_VEN, and SINUS) were used to regulate the changes during three phases (phase I: stages 1 to 3; phase II: stages 4 and 5; phase III: stage 6 and later) of petal development (Fig. 3, B and C). In phase I, BLA promoted the flattening of the distal part, whereas STK inhibited the flattening of the base, and thus, a nearly flat structure with a slightly narrow stalk was generated. In phase II, domains of AD and AB were redistributed according to the expression patterns of the examined adaxial and abaxial genes, and MID_VEN and MID_DOR were activated to promote the growth of the upper and lower lips, respectively. As a result, the upper lip was generated, and the entire petal became a stalked bilabiate structure with a clear *Querzone*. Last, in phase III, the growth inhibitor SINUS was invoked, so that a deep sinus was formed on the middle of lower

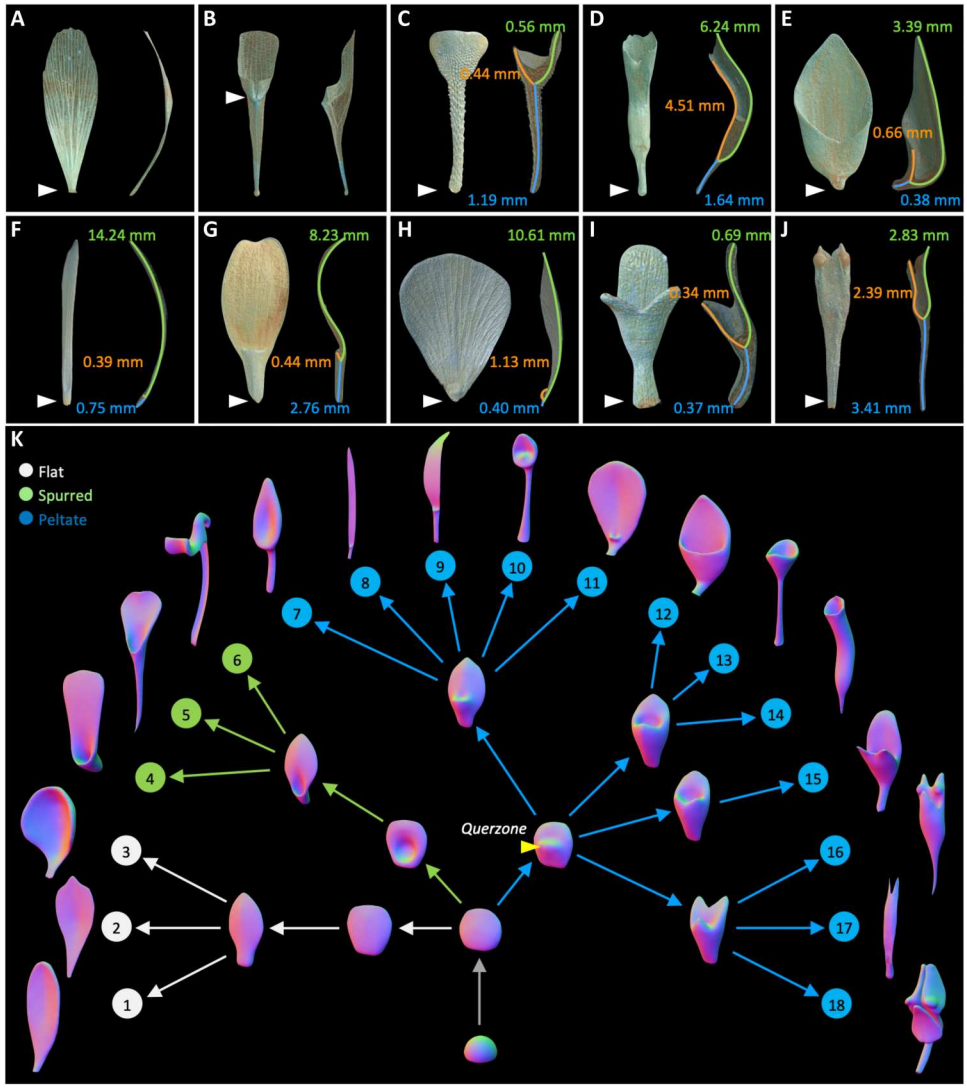

Fig. 1. Structures and diversification of ranunculaceous petals. (**A** to **J**) Front views and longitudinal sections [in micro–computed tomography (micro-CT)] showing the petals of 10 representative species: *Adonis sutchuenensis* (A), *Aquilegia viridiflora* (B), *Dichocarpum fargesii* (C), *Helleborus thibetanus* (D), *Isopyrum manshuricum* (E), *Trollius chinensis* (F), *Oxygraphis glacialis* (G), *Ranunculus japonicus* (H), *Leptopyrum fumarioides* (I), and *Eranthis stellata* (J). Green, blue, and orange lines mark the lengths of the lower lip, stalk, and upper lip, respectively, whereas white arrowheads mark the attached points of the petals on the receptacles. Measurements are given in the same colors as the lines. (**K**) Virtual clay models showing the trajectories of petal development in *A. sutchuenensis* (1), *Actaea asiatica* (2), *Anemonopsis macrophylla* (3), *Urophysa rockii* (4), *A. viridiflora* (5), *Aconitum kusnezoffii* (6), *Coptis japonica* (7), *T. chinensis* (8), *O. glacialis* (9), *Asteropyrum cavaleriei* (10), *R. japonicus* (11), *I. manshuricum* (12), *D. fargesii* (13), *H. thibetanus* (14), *L. fumarioides* (15), *E. stellata* (16), *N. integrifolia* (17), and *N. damascena* (18), as described (*4*, *5*, *21*, *22*). Yellow arrowhead points to the *Querzone*.

lip. The whole organ, then, resembles the basic structure of the *N. damascena* petal very much (Fig. 3, C and D).

To test the reliability of this model, we made a series of predictions and performed functional studies. Theoretically, if AD was removed from the petal primordium at the beginning of phase I, then a unifacial needle-like structure would be generated; if AD was removed at the beginning of phase II, then a structure with a cylindrical base and a flattened tip would be obtained; if AD was removed at the beginning of phase III, before SINUS was invoked but after AD and AB were redistributed, then a stalked structure with a small ventral lobe and an entire dorsal lobe would be obtained; if AD was removed after SINUS was invoked, then the resultant structure would be very similar to the wild-type petal (Fig. 3C). Similar predictions can be made when AB was removed at different stages of petal development, except that the resultant structures mirror the ones in which AD was removed (fig. S4). In reality, when the expression of the adaxially expressed *NidaPHX* (Fig. 3D and figs. S5 and S6), or the abaxially expressed miR166 (fig. S4), was knocked down by using the VIGS technique, a series of phenotypes resembling the predicted structures were obtained, suggesting that our model is reliable. Notably, while the petals from different VIGS treatments of the adaxial and abaxial genes showed very similar phenotypes, they were quite different at the cellular level, showing opposite internal polarity characteristics (fig.

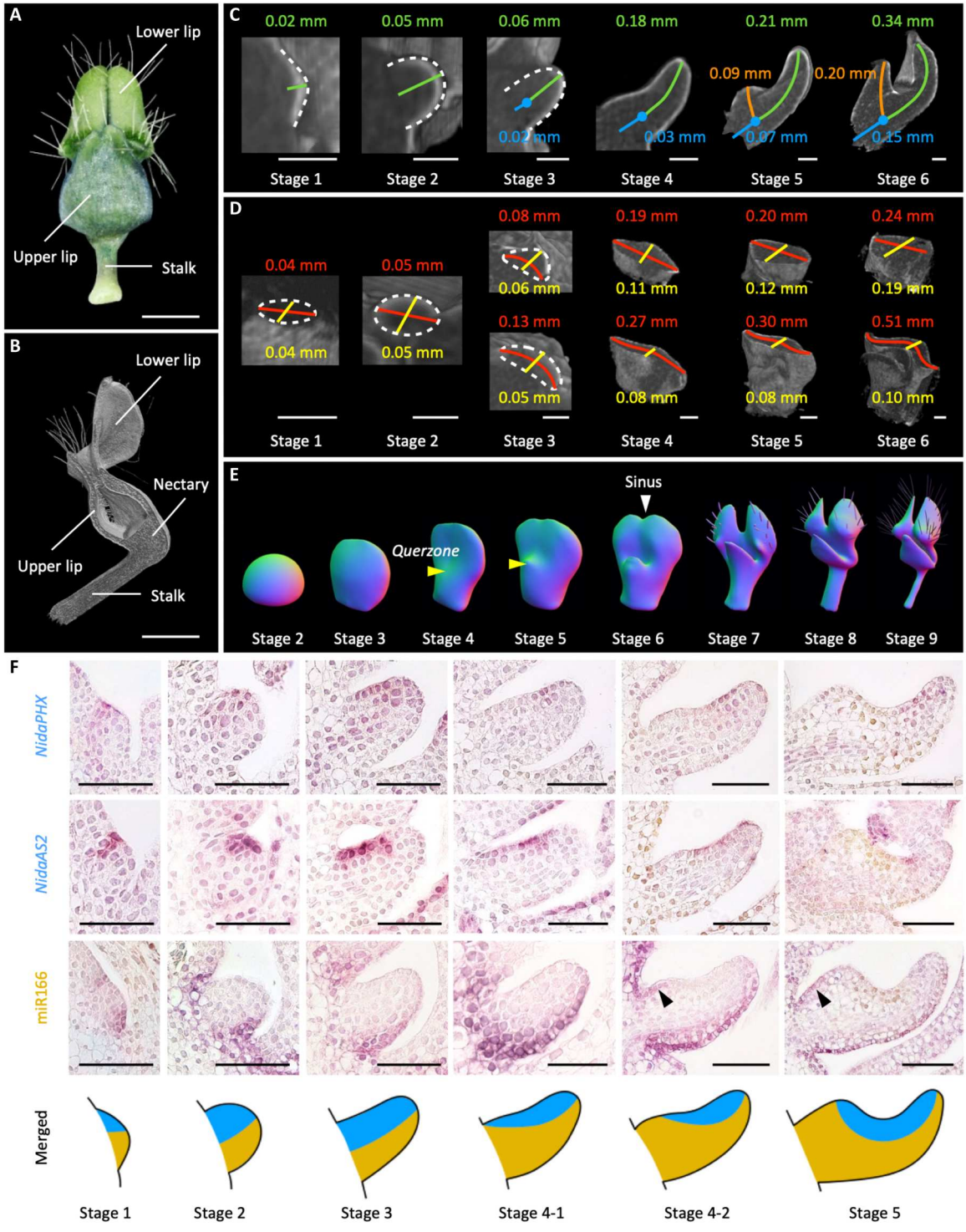

Fig. 2. Development of *Nigella damascena* petals and expression of key adaxial and abaxial genes. (**A** and **B**) Front view (A) and longitudinal section [(B); in micro-CT] of a mature petal of *N. damascena*, with the lower lip, upper lip, stalk, and nectary being marked. (**C** and **D**) Longitudinal (C) and transverse (D) sections (in micro-CT) of the petals at different developmental stages (1 to 6). In (C), green, blue, and orange lines mark the lengths of the lower lip, stalk, and upper lip, respectively. In (D), red lines mark the widths of the primordia (stages 1 and 2), the lower lips (the bottom row from stages 3 to 6), and the stalks (the top row from stages 3 to 6); yellow lines mark the thicknesses of the primordia (stages 1 and 2), the lower lips (the bottom row from stages 3 to 6), and the stalks (the top row from stages 3 to 6); white dotted lines mark the outlines of longitudinal and transverse sections of the primordia. Measurements are given in the same colors as the lines. (**E**) Successive virtual clay models showing the development of the *N. damascena* petals, with yellow arrowheads pointing to the *Querzone* and white arrowhead pointing to the sinus. (**F**) Expression patterns of *NidaPHX*, *NidaAS2*, and miR166 during petal development, with black arrowheads indicating the positions of the ectopic expression. In the merged diagram, the blue and brown areas represent the adaxial and abaxial domains, respectively. Scale bars, 100 μm in (A) and (B) and 50 μm in (C), (D), and (F).

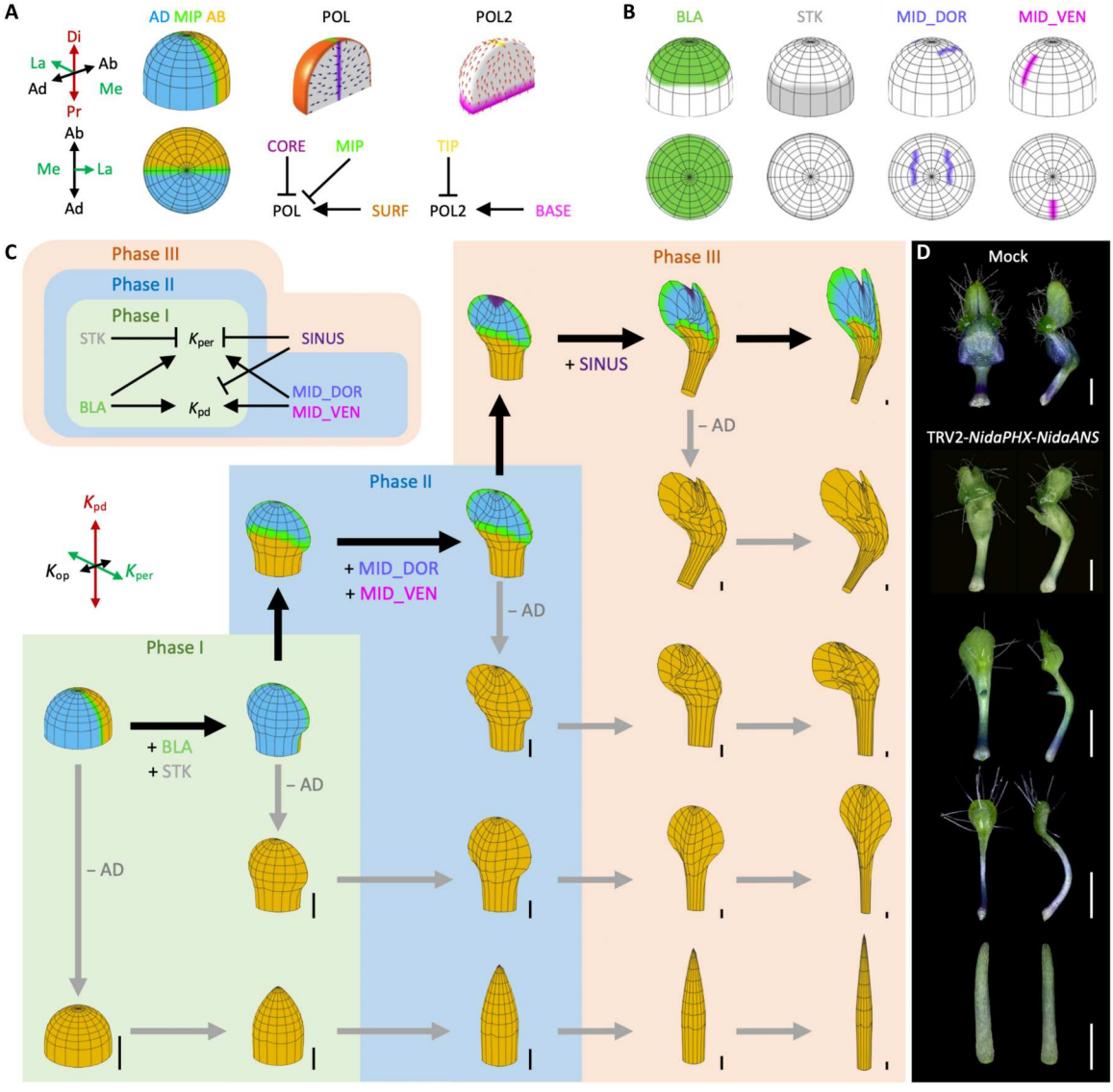

Fig. 3. Simulation of *N. damascena* petals and functional verification. (**A** and **B**) Initial setups of the model. Oblique and top views show the distributions of the factors used (i.e., AD, AB, MIP, BLA, STK, MID_DOR, and MID_VEN). Ad, adaxial; Ab, abaxial; Pr, proximal; Di, distal; Me, medial; La, lateral. POL (black arrows) runs from SURF toward MIP and CORE, whereas POL2 (red arrows) runs from BASE to the TIP. (**C**) Modeling process and the results. Patterns of growth in different phases (phases I to III) are determined by different growth rate regulatory networks: BLA and STK regulate the differential growth in phase I; MID_DOR and MID_VEN promote the expansion of local areas in phase II; and SINUS inhibits the local growth in phase III. Different final states are obtained when AD is removed from the beginning of different developmental phases. (**D**) Petals of the mock and those of TRV2-*NidaPHX-NidaANS*–treated plants with strong phenotypic changes. Scale bars, 100 μm.

S7). In addition, knocking down of other adaxial genes (i.e., *NidaHB8* and *NidaAS2*) (figs. S8 and S9) and an abaxial gene (i.e., *NidaARF3-2*) (fig. S10) also supports the model predictions.

Proposal of a simple and generalized modeling system

Notably, in our *N. damascena* model and the ones for carnivorous traps (*20*), the positions and ranges of AD and AB were defined separately and specifically, so that different models require different sets of parameters. To solve this problem and to simplify and generalize the modeling system, we proposed three parameters, L, θ, and H, to describe the relative positions of AD and AB domains. Here, L refers to the distance between the midplane of AD/AB and the center of the hemispheric tip of the organ primordium, θ refers to the angle between the normal of the midplane and the base of the hemispheric tip of the organ primordium, and H refers to the height of the primordium base (Fig. 4A). Theoretically, the value of H roughly reflects the time when AD and AB start to shift: A larger value means a later shift on the primordium with a longer stalk. Note that the three parameters collectively reflect an equilibrium state of the AD/AB boundary rather than a single gene or molecular component. When L, θ, and H were all set to 0, the distributions of AD and AB were equal and the midplane coincided with that of the organ primordium. In this case, setting K_{op} much smaller than K_{pd} and K_{per} would lead to the generation of a flat sheet equivalent to the conventional bifacial leaves.

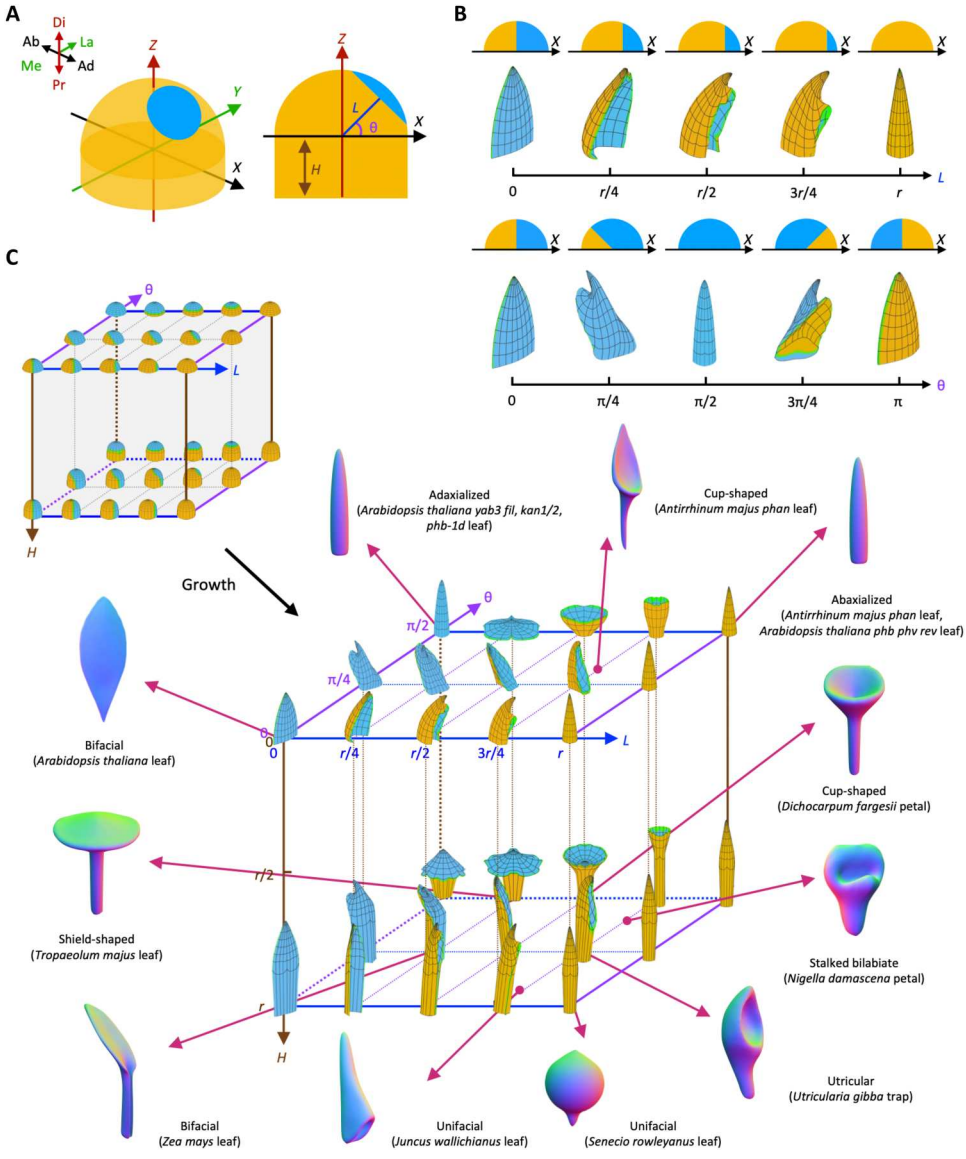

Fig. 4. A simple and generalized modeling system for simulating various basic shapes. (**A**) Schematic diagrams (oblique and sagittal section views) showing the parameters of the initial model. *L* refers to the distance between the original point (0, 0, 0) of the coordinate system and the midplane of AD and AB domains, θ refers to the angle between the normal of the midplane and *X*-*Y* plane (*Z* = 0), and *H* refers to the height of the cylindrical base. (**B**) Initial (section view) and final states (oblique view) of the models by increasing the values of parameter *L* (from 0 to *r*) or θ (from 0 to π). *r* is the radius of the hemispheric tip of the primordium. (**C**) Three-dimensional morphospaces showing the initial and final states of the models by changing the values of *L* (from 0 to *r*), θ (from 0 to π/2), and *H* (from 0 to *r*). Representative organs resembling the corresponding shapes are presented with virtual clay models.

When *L* was set to a positive value (e.g., *r*/4, *r*/2, 3*r*/4, or *r*, where *r* is the radius of the hemispheric tip of the primordium) whereas θ, *H*, K_{op}, K_{pd}, and K_{per} remained unchanged, the midplane would shift toward the adaxial side of the primordium. In this case, the resultant structures would vary from a pointed, slightly curved bifacial sheet to a totally abaxialized unifacial cone (Fig. 4B), resembling the needle-like leaves of the *Antirrhinum majus phan* mutant (*9*) and the *Arabidopsis thaliana phv phb rev* mutant (*16*). When θ was set to a positive value (e.g., π/4 or π/2) whereas all other parameters remained unchanged, the midplane would rotate toward the abaxial side, leading to a series of states from distorted bifacial with a unifacial tip to adaxialized unifacial cone (Fig. 4B), the latter of which resembles the leaves of the *A. thaliana kan1 kan2* and *yab3 fil* mutants, and the *phb-1d* dominant mutant (*13*–*16*). When θ increased further (i.e., from π/2 via 3π/4 to π), structures with reversed AD and AB domains were generated, one state of which resembles the inverted leaves of the *A. thaliana CLAVATA3::KAN1* plants (*29*).

When the values of *L*, θ, and *H* were all adjusted, a 3D morphospace was formed (Fig. 4C and fig. S11), in which many subtypes of peltate structures were included. For example, when *L* = *r*/4, θ = π/2, and *H* = *r*, a structure with an abaxialized cylindrical base and a bifacial blade was generated, resembling the shield-shaped leaves of *T. majus* (*18*). When *L* = 3*r*/4, θ = π/4, and *H* = *r*, a tilted cup-shaped

structure was formed, similar to the utricular traps of *U. gibba* (*20*). If $L = r/2$, $\theta = \pi/2$, and $H = r$, then an upright cup-shaped model, resembling the petals of *D. fargesii*, was generated. Meanwhile, in a mirrored morphospace (fig. S11E) where AD and AB were switched, hypopeltate structures resembling leaves of the *A. thaliana phb-1d* mutants (*8*) and some natural species [e.g., bracts of *Pelargonium* (Geraniaceae) species and leaves of *Ficus krishnae* (Moraceae)] (*30*) can be formed. In addition to the formation of different peltate forms, a variety of bifacial and unifacial structures, such as the sheathing leaves of maize (*31*) and terete leaves of *Juncus wallichianus* (Juncaceae) (*32*), also emerged in this morphospace.

Simulation of the peltate petals in other ranunculaceous species

Although many peltate structures have been included in the *L*-θ-*H* morphospace, few of them resemble the real peltate petals of some ranunculaceous species very well. To solve this problem, we reinvestigated the morphological and developmental data of ranunculaceous petals (Fig. 1) and found that factors affecting the length of the stalk and the relative sizes of the upper and lower lips are the key to the diversification of peltate petals within the Ranunculaceae. For this reason, we chose a cup-shaped structure ($L = 3r/4$, $\theta = \pi/2$, and $H = r/2$) within the *L*-θ-*H* morphospace as the ground state and used the three regional growth factors (e.g., BLA, STK, and MID, the coefficients of which on K_{pd} are P_{bla}, P_{stk}, and P_{mid}, respectively) to regulate the growth of the petal in different parts (Fig. 5, A to C). As a result, goblet-shaped structures with different lengths of stalks were generated when the value of P_{stk} was increased, whereas tubular ones with different lengths of lobes were created when the value of P_{bla} was enhanced (Fig. 5D). In addition, when the values of P_{stk}, P_{bla}, and P_{mid} were changed simultaneously, another 3D morphospace was formed, in which structures resembling the peltate petals of most ranunculaceous species were included (Fig. 5E). Clearly, addition of these three parameters has improved the effectiveness of the simulation.

Notably, despite the effectiveness of the modeling system, there are still petals that have not been simulated. Specifically, petals of *Leptopyrum fumarioides* and *Eranthis stellata*, which have a sinus on the upper and lower lips, respectively, are missing from the second morphospace. To solve this problem, we divided the growth-promoting factor MID into MID_DOR and MID_VEN and added the growth-inhibiting factor SINUS when necessary (Fig. 5, F, G, and I). As a result, structures resembling petals of both *L. fumarioides* (Fig. 5H) and *E. stellata* (Fig. 5J) were generated. Meanwhile, by adjusting the values of more parameters (i.e., P_{bla}, P_{stk}, P_{mid_dor}, P_{mid_ven}, and P_{sinus}), structures resembling the petals of other *Nigella* species were generated (Fig. 5, K and L). Petals of *Nigella integrifolia*, for example, were produced by increasing the value of P_{mid_dor} (from 0.4 to 2.0) and P_{stk} (from 0.4 to 0.5) and decreasing the values of P_{bla} (from 0.65 to 0), whereas those of *Nigella nigellastrum* by increasing the value of P_{mid_dor} (from 0.4 to 1.5) and P_{mid_ven} (from 0.25 to 0.8) and decreasing the values of P_{bla} (from 0.65 to 0). Because the changes in the modeling system are also consistent with the way of petal diversification within the genus *Nigella* (*21*), it is very likely that our modeling system can help or guide the understanding of the processes that cannot be witnessed.

Simulation of structures with spurs, pouches, ruffles, and marginal modifications

Although various bifacial, unifacial, and peltate structures have been included in the aforementioned morphospaces, there are still ranunculaceous petals that cannot be simulated using the available parameters. To solve this problem and to simulate structures with spurs, pouches, ruffles, and other types of marginal modifications, we introduced an additional growth factor, ADD, to promote additional regional growth. When ADD was set to promote the growth in the center of a flat, bifacial primordium, spurred and pouched structures resembling petals of *Aquilegia* and *Paphiopedilum* (Orchidaceae), respectively, were produced (fig. S12, A to C). When ADD was set to promote the growth in the peripheral areas of the primordium, structures similar to the ruffled petals of *Lagerstroemia indica* (Orchidaceae) were generated (fig. S12D). When ADD was set to promote the growth of only one side of the primordium, organs with oblique, bilaterally asymmetrical bases, like the ventral (rather than dorsal or lateral) sepals of *Delphinium* and leaves of *Begonia* (Begoniaceae) (*33*), were generated (fig. S12, E and F).

If ADD was used together with SINUS, then organs with more sophisticated regional modifications can be simulated (fig. S13) (*34*). For instance, when ADD was set to be distributed alternately with SINUS along the margin, with the values of the coefficients P_{add_pd} and P_{add_per} being set to 4, rounded protrusions resembling lobes of lobed leaves emerged (fig. S13, A and B). When the values of P_{sinus} (from 0 to 20), P_{add_per} (from 0 to 4), and P_{add_pd} (from 0 to 10) were fine-tuned further, another 3D morphospace formed, in which various types of marginal elaborations were included (fig. S13C). When P_{add_pd} was set equal to P_{add_per} (i.e., $P_{add\_pd} = P_{add\_per} = 1$), repeated protrusions were formed, resembling the serrations along the margins of *A. thaliana* leaves (*35*). If the value of P_{add_pd} was set much greater than P_{add_per} ($P_{add\_pd} = 10$, $P_{add\_per} = 0$), then filiform outgrowths similar to the tendrils, tentacles, or fringes of leaves were generated. When the distributions of ADD and SINUS, as well as the values of coefficients (P_{add_pd}, P_{add_per}, and P_{sinus}), were all adjusted, structures resembling diverse compound leaves were created (Fig. 6 and figs. S13, D to G, and S14) (*36*).

DISCUSSION

The applicability and reliability of the modeling system

Computational modeling has increasingly been used to understand the mechanisms underlying the development of plant lateral organs (*37*). Modeling systems (e.g., L-system and vertex models) that take into account the mechanical stresses and/or auxin dynamics, for example, have been developed to simulate diverse simple and compound leaves (*38*, *39*). A polarity-based modeling system, which solves the problems of growth in 3D, has not only simulated the volumetric growth of bifacial and sheathing leaves but also uncovered the mechanisms underlying the formation of carnivorous traps (*20*, *31*). The problem, however, is that the positions and ranges of AD and AB were defined separately and specifically, so that different models require different sets of parameters. In this study, by introducing only three parameters (*L*, θ, and *H*) to depict the relative positions of AB and AD and few factors to reflect the position, direction, and degree of regional growth, we propose a simple yet greatly generalized polarity-based modeling system (Fig. 6 and movies S1 to S16). The system, in turn, not only helped us successfully simulate the formation of various bifacial, unifacial, and peltate

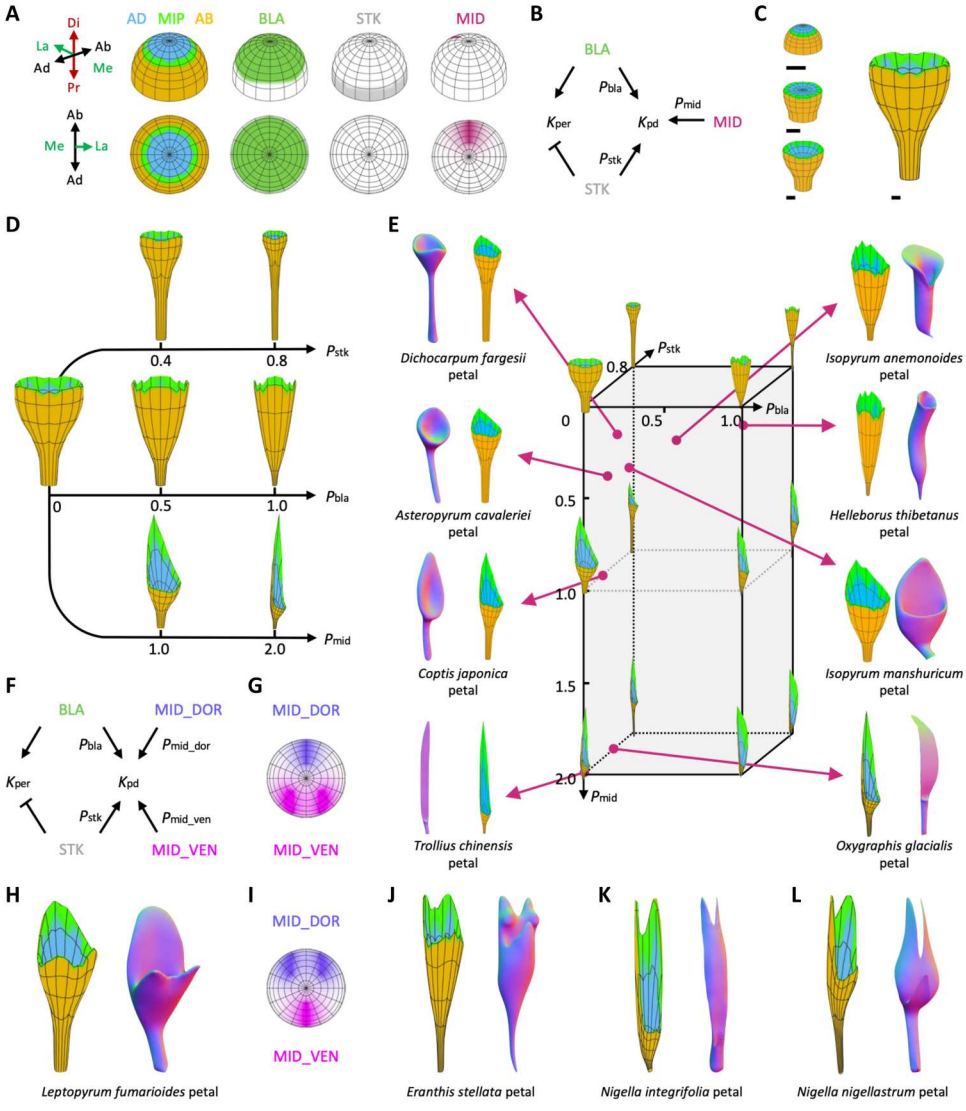

Fig. 5. Simulation of the diverse peltate petals within the Ranunculaceae. (**A**) Oblique and top views showing the distributions of the factors used (i.e., AD, AB, MIP, BLA, STK, and MID). (**B**) Growth rate regulatory network (KRN) of the model. (**C**) Developmental stages of the model when $P_{stk} = 0$, $P_{bla} = 0$, and $P_{mid} = 0$. Scale bars are in arbitrary units. (**D**) Final states of the models by changing the values of P_{stk} (0.4, 0.8), P_{bla} (0.5, 1.0), and P_{mid} (1.0, 2.0), respectively. (**E**) Resultant morphospace showing the final states of the models. Representatives of different subtypes of peltate petals are presented with virtual clay models. (**F** to **L**) Models of peltate petals with marginal elaborations. In the modified KRN, MID is replaced by MID_DOR and MID_VEN (F). Distributions of MID_DOR and MID_VEN (top view) are shown in (G) and (I), and the final states of the models, which correspond to the petals of four ranunculaceous species, are shown in (H) and (J) to (L).

structures but also allowed us to explore the important issues regarding the diversification of plant lateral organs in shape (e.g., what determines the exact positions and ranges of AD and AB domains, and why is the distribution of real forms in a morphospace uneven?) Clearly, simplification and generalization of the modeling system have substantially increased its applicable scope.

In addition to its wide applicability, the modeling system is also very reliable, with the resultant models being well supported by, or at least largely consistent with, real data. Despite the lack of functional studies, the distributions of AD and AB in our models, for example, are consistent with the expression patterns of adaxial and abaxial genes in bifacial, unifacial, or peltate leaves/petals in *A. thaliana*, *A. majus*, *J. wallichianus*, *T. majus*, *U. gibba*, and *S. purpurea* (*8*, *9*, *18*–*20*, *32*). Meanwhile, when the *N. damascena* adaxial (i.e., *NidaPHX*, *NidaHB8*, and *NidaAS2*) and the abaxial (i.e., miR166 and *NidaARF3-2*) genes were knocked down separately or in a combinational manner, a series of phenotypes resembling the predicted morphologies were obtained (Fig. 3D and figs. S4 to S10), suggesting that the models are very reliable.

Molecular bases of the polarity shifts and differential growths

The observation that shifts in adaxial-abaxial gene expression can cause peltation and other nonplanar deformation of lateral organs raises the question of how that could occur genetically. One possible reason, of course, is the regulatory changes of the polarity genes per se. Abundant evidence has shown that mutation, ectopic, or overexpression of adaxial-abaxial genes can lead to the production of

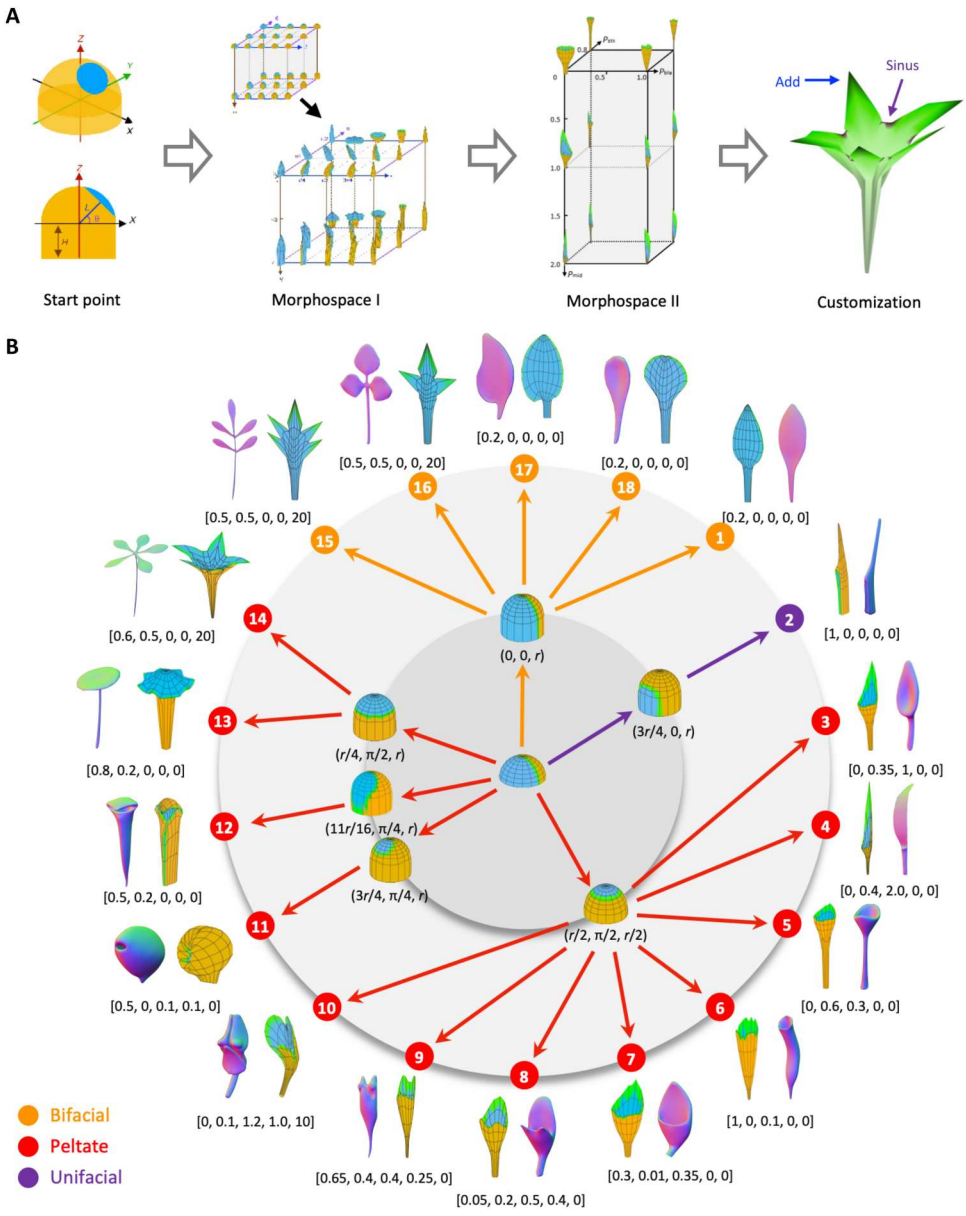

Fig. 6. Generation of diverse plant lateral organs with a generalized modeling system. (**A**) Hierarchical nature of the modeling system. (**B**) Modeling of plant lateral organs with various basic shapes and marginal modifications within the generalized modeling system. The inner circle shows the changes from a start point (i.e., a hemispheric bifacial primordium) to various intermediate states by adjusting the values of *L*, θ, and *H* (in round brackets). The outer circle shows the changes from various intermediate states to more final states by adjusting the values of P_{bla}, P_{stk}, P_{mid_dor}, P_{mid_ven}, and P_{sinus} (in square brackets). Real examples of the final states include the following: the simple bifacial leaf of *A. thaliana* (1); the unifacial leaf of *J. wallichianus* (2); the peltate petals of *C. japonica* (3), *O. glacialis* (4), *D. fargesii* (5), *H. thibetanus* (6), *I. manshuricum* (7), *L. fumarioides* (8), *E. stellata* (9), and *N. damascena* (10); the utricular traps of *U. gibba* (11); the pitcher-shaped leaf of *Sarracenia flava* (12); the shield-shaped leaf of *T. majus* (13); the peltately palmate compound leaf (14); the pinnate compound leaf (15); the ternately compound leaf (16); the asymmetrical leaf (17); and the simple petal (18).

radialized, lotus-shaped, or cup-shaped leaves (*8*). Moreover, of the adaxial and abaxial genes investigated so far, homologs of the HD-ZIP III family genes appear to be hotspots because formation of traps in *U. gibba*, pitcher leaves in *S. purpurea*, unifacial leaves in *J. wallichianus*, stamens in *Oryza sativa*, and peltate petals in *N. damascena* were all caused by, or at least related to, shifts in their expression (*18*–*20*, *32*, *40*). Nevertheless, external factors, such as the hypothesized Sussex signal, may also be involved, because perturbation of them can break the balance of adaxial-abaxial polarity and thus result in the generation of nonplanar leaves (*41*, *42*). In addition, in at least a few species (e.g., *N. damascena*), the adaxial-abaxial network seems to be regulated by the petal identity determination program because inactivation of the petal identity gene (e.g., *NidaAPETALA3-3*) can lead to the conversion of the originally peltate petals into bifacial sepal-like structures (*43*). Moreover, recent studies have shown that shifts in the adaxial-

abaxial system are regulated by the direct threshold-based readout of mobile RNA gradients (*44*) and/or the coordination of different polarity systems (*45*).

In addition to the factors that specify the distributions of adaxial and abaxial domains, there are genes that likely function as the regional growth factors. *BLADE-ON-PETIOLE 1* (*BOP1*), whose homologs in *A. thaliana*, barley, rice, and maize regulate meristematic activity in a proximodistally dependent manner in leaves or floral organs (*31*, *46*, *47*), for example, may be a candidate gene of STK, which regulates the formation of stalk, petiole, claw, or sheath in various organs through inhibiting the lateral expansion at the proximal part of the primordium. Consistent with the activity of STK, the *NidaBOP1* gene in *N. damascena* was also expressed in the basal part of the petal primordia (fig. S15). Similarly, SINUS, a factor that determines marginal elaborations by inhibiting regional growths, may have something to do with *REDUCED COMPLEX* (*RCO*)/*LATE MERISTEM IDENTITY1* (*LMI1*) and/or *CUP-SHAPED COTYLEDON1* (*CUC1*), homologs of which have been reported to regulate the formation of serrates, lobes, or leaflets by inhibiting the rate of cell division (*24*, *35*, *48*–*50*). For MID, BLA, and ADD, the available data suggest that regulators controlling blade expansion, meristematic activities, or plant hormones may be the key (*51*–*53*), although more studies are needed to reveal the molecular bases of these factors.

The uneven distribution of real forms in the morphospaces

It has been widely accepted that morphospaces, which describe the realms of possible morphologies in theoretical spaces, are usually unevenly populated by actual forms (*54*). The three major types of inflorescences (i.e., panicles, racemes, and cymes) of flowering plants, for example, only occupy a small region of a multidimensional space (*55*). In animals, the coiled shells are just concentrated in a corner of the famous Raup's morphospace (*56*), suggestive of uneven distribution. In this study, we have shown that the distributions of diverse lateral organs in the morphospaces are also strongly biased. In the adaxial-abaxial morphospace formed by *L*, θ, and *H*, the three main forms (i.e., bifacial, unifacial, and peltate) of lateral organs present in nature are all restricted in the region where the values of θ are no more than π/2 (Fig. 4C). In addition, while the forms observed in the adaxial-abaxial mutants can sometimes take up more areas than those in the wild type, the entire space is still not fully occupied. In the morphospace specifically constructed for petals of the ranunculaceous species (i.e., the one formed by P_{bla}, P_{stk}, and P_{mid}), peltate petals of various types tend to be located around the vertex where the values of P_{bla}, P_{stk}, and P_{mid} are all very small (Fig. 5E).

Theoretically, the uneven distribution of real forms in a morphospace may be attributed to developmental constraint or natural selection, or both (*54*). In the adaxial-abaxial morphospace formed by *L*, θ, and *H*, the developmental constraint imposed by the prepatterning (θ = 0) of the adaxial-abaxial identities appears to be critical for shaping the distribution pattern of the three basic types of organ shapes. Specifically, while breaking or alternating this constraint can create diverse nonplanar shapes, it is hard for the prepatterning to be reversed (i.e., θ = π) in natural states, and this explains the reason why the actual shapes are only restricted to one side (θ ≤ π/2, but not θ > π/2) of the morphospace. In addition, mechanical stresses, especially those that limit the expansion and/or proliferation of cells, can become the developmental constraint that prevents the overgrowth of organs (*57*). Nevertheless, natural selection may also be in action, through which the preferred forms (e.g., cup-shaped leaves or petals) were retained, whereas the nonpreferred ones (e.g., adaxialized leaves) were eliminated. The lack of extremely long blades in peltate petals, for example, may have been restricted by the proboscis lengths of pollinators (*58*). Whatever the reason is, our generalized modeling system can act as a framework to understand the genetic and developmental mechanisms underlying plant evolution.

MATERIALS AND METHODS

Plant material

Seeds of *N. damascena* were sown in 2:1 mixed roseite and nutrient soil and grown under conditions of 12-hour day/night at 24°C and 60% relative humidity.

Imaging and image processing

High-resolution 3D images of fresh petals at different developmental stages were taken in a micro–computed tomography (micro-CT) scanner (Bruker SkyScan 1172, Germany) as described (*21*). Image stacks were aligned using NRecon v.1.6 for 3D reconstruction, and visualization and measurement of reconstructed images were made using VolViewer (https://cmpdartsvr3.cmp.uea.ac.uk/wiki/BanghamLab/index.php/VolViewer) and Fiji (https://fiji.sc/) (*59*), respectively. For each developmental stage, morphological parameters of three different petals were measured (table S1). Flowers and petals were dissected and then photographed with a digital microscope Leica DVM6 for morphological observation or imaged by a scanning electron microscope HitachiS-4800 field-emission scanning electron microscope for cellular observation. In addition, paraffin and semithin section series of the petals and toluidine blue staining were performed for histological observation. Serial sections were photographed using a Leica DM5000 B microscope (Leica, Wetzlar, Germany) as described (*21*, *25*).

Phylogenetic analysis

Coding sequences of the genes from *N. damascena* and other species were retrieved through BLAST searches against publicly available databases. Sequence alignment and adjustment were conducted as described (*60*). The alignable nucleotide matrix was used for phylogenetic reconstruction in IQ-TREE 1.6.10 (*61*) with the maximum-likelihood method. The best-fit models were chosen using ModelFinder (*62*), and 1000 bootstrap replicates were performed. Genes isolated from this study were named according to their phylogenetic belongingness and sequence features.

In situ hybridization

mRNA in situ hybridization was performed to investigate the expression patterns of *NidaPHX*, *NidaHB8*, *NidaAS2*, *NidaYAB5*, and *NidaBOP1* following the procedure as described (*21*). Detection of miR166 was performed by using the miR166 complementary locked nucleic acid (LNA)–modified DNA probes, while Scramble-miRCURY LNA Detection probe was used as a negative control. For the LNA probe, hybridization was performed at 55°C and the probe concentration was 10 nM (*63*). The primers used are listed in table S2.

Functional study

For VIGS, gene-specific fragments of *NidaPHX*, *NidaHB8*, *NidaAS2*, *NidaARF3-2*, and *Nida ANTHOCYANIDIN SYNTHASE* (*NidaANS*) were amplified and introduced into the tobacco rattle virus 2 (TRV2)–based pYL156 vector to generate the constructs (*23*). For knocking down of miR166, a short tandem target mimic (STTM) system was used and the STTM166 sequence was synthesized (*64*), amplified, and introduced into the TRV2-based pYL156 vector. The fragment of *NidaANS* gene was added as an indicator, because silencing of it can cause the loss of anthocyanidin of the flower. At least 360 plants were treated for each construct before the differentiation of flower buds. Phenotypes of petals were observed at the mature stage and categorized on the basis of their morphological features. The efficiency of the silencing was checked by quantitative reverse transcription PCR (qRT-PCR) as described (*23*). The primers used for VIGS and qRT-PCR are listed in table S3.

Computational modeling

All virtual clay models of different leaves and petals were made by using Sculptris (https://doi.org/10.1038/s41551-022-00968-1). Virtual clay models of *N. damascena* petals at different stages were produced on the basis of the micro-CT data. All computational models were performed with MATLAB (https://www.mathworks.com/products/matlab.html) and an implemented toolbox, *GFtbox* (https://github.com/JIC-Enrico-Coen/GrowthToolbox). Code is available at the GitHub repository (https://github.com/Darwincj/GFtbox_peltate_organs) and in the Supplementary Materials (data S1). Details of the modeling are described in the Supplementary Materials.

Supplementary Materials

This PDF file includes:
Supplementary Text
Figs. S1 to S15
Tables S1 to S3
Legends for movies S1 to S16
Legend for data S1

Other Supplementary Material for this manuscript includes the following:
Movies S1 to S16
Data S1

View/request a protocol for this paper from *Bio-protocol*.

REFERENCES AND NOTES

1. D. Franck, The morphological interpretation of epiascidiate leaves—An historical perspective. *Bot. Rev.* **42**, 345–388 (1976).
2. W. Troll, Morphologie der schieldförmigen blätter. *Planta* **17**, 153–230 (1932).
3. C. Thorogood, U. Bauer, S. Hiscock, Convergent and divergent evolution in carnivorous pitcher plant traps. *New Phytol.* **217**, 1035–1041 (2018).
4. C. Erbar, S. Kusma, P. Leins, Development and interpretation of nectary organs in Ranunculaceae. *Flora* **194**, 317–332 (1999).
5. K. Kosuge, Petal evolution in Ranunculaceae. *Plant Syst. Evol.* **8**, 185–191 (1994).
6. C. Darwin, *Insectivorous Plants* (London, 1875).
7. D. Franck, Early histogenesis of the adult leaves of *Darlingtonia californica* (Sarraceniaceae) and its bearing on the nature of epiascidiate foliar appendages. *Am. J. Bot.* **62**, 116–132 (1975).
8. K. Fukushima, M. Hasebe, Adaxial-abaxial polarity: The developmental basis of leaf shape diversity. *Genesis* **52**, 1–18 (2014).
9. R. Waites, A. Hudson, *phantastica*: A gene required for dorsoventrality of leaves in *Antirrhinum majus*. *Development* **121**, 2143–2154 (1995).
10. M. Byrne, R. Barley, M. Curtis, J. M. Arroyo, M. Dunham, A. Hudson, R. A. Martienssen, *Asymmetric leaves1* mediates leaf patterning and stem cell function in *Arabidopsis*. *Nature* **408**, 967–971 (2000).
11. J. McConnell, J. Emery, Y. Eshed, N. Bao, J. Bowman, M. Barton, Role of *PHABULOSA* and *PHAVOLUTA* in determining radial patterning in shoots. *Nature* **411**, 709–713 (2001).
12. F. T. S. Nogueira, S. Madi, D. H. Chitwood, M. Juarez, M. C. P. Timmermans, Two small regulatory RNAs establish opposing fates of a developmental axis. *Genes Dev.* **21**, 750–755 (2007).
13. K. R. Siegfried, Y. Eshed, S. F. Baum, D. Otsuga, G. N. Drews, J. L. Bowman, Members of the *YABBY* gene family specify abaxial cell fate in *Arabidopsis*. *Development* **126**, 4117–4128 (1999).
14. I. Pekker, J. Alvarez, Y. Eshed, Auxin response factors mediate *Arabidopsis* organ asymmetry via modulation of KANADI activity. *Plant Cell* **17**, 2899–2910 (2005).
15. R. Kerstetter, K. Bollman, R. A. Taylor, K. Bomblies, R. S. Poethig, *KANADI* regulates organ polarity in *Arabidopsis*. *Nature* **411**, 706–709 (2001).
16. J. Emery, S. K. Floyd, J. Alvarez, Y. Eshed, N. P. Hawker, A. Izhaki, S. F. Baum, J. L. Bowman, Radial patterning of *Arabidopsis* shoots by class III HD-ZIP and KANADI genes. *Curr. Biol.* **13**, 1768–1774 (2003).
17. M. T. Juarez, J. S. Kui, J. Thomas, B. A. Heller, M. C. P. Timmermans, microRNA-mediated repression of *rolled leaf1* specifies maize leaf polarity. *Nature* **428**, 84–88 (2004).
18. S. Gleissberg, E. P. Groot, M. Schmalz, M. Eichert, A. Kölsch, S. Hutter, Developmental events leading to peltate leaf structure in *Tropaeolum majus* (Tropaeolaceae) are associated with expression domain changes of a YABBY gene. *Dev. Genes Evol.* **215**, 313–319 (2005).
19. K. Fukushima, H. Fujita, T. Yamaguchi, M. Kawaguchi, H. Tsukaya, M. Hasebe, Oriented cell division shapes carnivorous pitcher leaves of *Sarracenia purpurea*. *Nat. Commun.* **6**, 6450 (2015).
20. C. D. Whitewoods, B. Gonçalves, J. Cheng, M. Cui, R. Kennaway, K. Lee, C. Bushell, M. Yu, C. Piao, E. Coen, Evolution of carnivorous traps from planar leaves through simple shifts in gene expression. *Science* **367**, 91–96 (2020).
21. X. Yao, W. Zhang, X. Duan, Y. Yuan, R. Zhang, H. Shan, H. Kong, The making of elaborate petals in *Nigella* through developmental repatterning. *New Phytol.* **223**, 385–396 (2019).
22. P. Delpeuch, F. Jabbour, C. Damerval, J. Schönenberge, S. Pamperl, M. Rome, S. Nadot, A flat petal as ancestral state for Ranunculaceae. *Front. Plant Sci.* **13**, 961906 (2022).
23. P. Wang, H. Liao, W. Zhang, X. Yu, R. Zhang, H. Shan, X. Duan, X. Yao, H. Kong, Flexibility in the structure of spiral flowers and its underlying mechanisms. *Nat. Plants* **2**, 15188 (2016).
24. R. Zhang, X. Fu, C. Zhao, J. Cheng, H. Liao, P. Wang, X. Yao, X. Duan, Y. Yuan, G. Xu, E. Kramer, H. Shan, H. Kong, Identification of the key regulatory genes involved in elaborate petal development and specialized character formation in *Nigella damascena* (Ranunculaceae). *Plant Cell* **32**, 3095–3112 (2020).
25. H. Liao, X. Fu, H. Zhao, J. Cheng, R. Zhang, X. Yao, X. Duan, H. Shan, H. Kong, The morphology, molecular development and ecological function of pseudonectaries on *Nigella damascena* (Ranunculaceae) petals. *Nat. Commun.* **11**, 1777 (2020).
26. E. Kramer, S. Hodges, *Aquilegia* as a model system for the evolution and ecology of petals. *Philos. Trans. R. Soc. Lond B Biol. Sci.* **365**, 477–490 (2010).
27. L. Zhao, P. Liu, X. Che, W. Wang, Y. Ren, Floral organogenesis of *Helleborus thibetanus* and *Nigella damascena* (Ranunculaceae) and its systematic significance. *Bot. J. Linn. Soc.* **166**, 431–443 (2011).
28. R. Kennaway, E. Coen, Volumetric finite-element modelling of biological growth. *Open Biol.* **9**, 190057 (2019).
29. M. P. Caggiano, X. Yu, N. Bhatia, A. Larsson, H. Ram, C. Ohno, P. Sappl, E. M. Meyerowitz, H. Jönsson, M. G. Heisler, Cell type boundaries organize plant development. *eLife* **6**, e27421 (2017).
30. P. Dupuy, M. Guédès, Hypoascidiate bracts in *Pelargonium*. *Bot. J. Linn. Soc.* **78**, 117–121 (1979).
31. A. E. Richardson, J. Cheng, R. Johnston, R. Kennaway, B. R. Conlon, A. B. Rebocho, H. Kong, M. J. Scanlon, S. Hake, E. Coen, Evolution of the grass leaf by primordium extension and petiole-lamina remodeling. *Science* **374**, 1377–1381 (2021).
32. T. Yamaguchi, S. Yano, H. Tsukaya, Genetic framework for flattened leaf blade formation in unifacial leaves of *Juncus prismatocarpus*. *Plant Cell* **22**, 2141–2155 (2010).
33. C. Martinez, D. Chitwood, R. Smith, N. Sinha, Left–right leaf asymmetry in decussate and distichous phyllotactic systems. *Philos. Trans. R. Soc. Lond B Biol. Sci.* **371**, 20150421 (2016).
34. A. Runions, M. Tsiantis, P. Prusinkiewicz, A common developmental program can produce diverse leaf shapes. *New Phytol.* **216**, 401–418 (2017).
35. G. D. Bilsborough, A. Runions, M. Barkoulas, H. W. Jenkins, A. Hasson, C. Galinha, P. Laufs, A. Hay, P. Prusinkiewicz, M. Tsiantis, Model for the regulation of *Arabidopsis thaliana* leaf margin development. *Proc. Natl. Acad. Sci. U.S.A.* **108**, 3424–3429 (2011).

36. M. Bar, N. Ori, Compound leaf development in model plant species. *Curr. Opin. Plant Biol.* **23**, 61–69 (2015).
37. N. Bhatia, A. Runions, M. Tsiantis, Leaf shape diversity: From genetic modules to computational models. *Annu. Rev. Plant Biol.* **72**, 325–356 (2021).
38. D. Kierzkowski, A. Runions, F. Vuolo, S. Strauss, R. Lymbouridou, A.-L. Routier-Kierzkowska, D. Wilson-Sánchez, H. Jenke, C. Galinha, G. Mosca, Z. Zhang, C. Canales, R. Ioio, P. Huijser, R. Smith, M. Tsiantis, A growth-based framework for leaf shape development and diversity. *Cell* **177**, 1405–1418.e17 (2019).
39. F. Zhao, F. Du, H. Oliveri, L. Zhou, O. Ali, W. Chen, S. Feng, Q. Wang, S. Lü, M. Long, R. Schneider, A. Sampathkumar, C. Godin, J. Traas, Y. Jiao, Microtubule-mediated wall anisotropy contributes to leaf blade flattening. *Curr. Biol.* **30**, 3972–3985.e6 (2020).
40. T. Toriba, T. Suzaki, T. Yamaguchi, Y. Ohmori, H. Tsukaya, H.-Y. Hirano, Distinct regulation of adaxial-abaxial polarity in anther patterning in rice. *Plant Cell* **22**, 1452–1462 (2010).
41. I. Sussex, Experiments on the cause of dorsiventrality in leaves. *Nature* **167**, 651–652 (1951).
42. J. Qi, Y. Wang, T. Yu, A. Cunha, B. Wu, T. Vernoux, E. Meyerowitz, Y. Jiao, Auxin depletion from leaf primordia contributes to organ patterning. *Proc. Natl. Acad. Sci. U.S.A.* **111**, 18769–18774 (2014).
43. R. Zhang, C. Guo, W. Zhang, P. Wang, L. Li, X. Duan, Q. Du, L. Zhao, H. Shan, S. Hodges, E. Kramer, Y. Ren, H. Kong, Disruption of the petal identity gene *APETALA3-3* is highly correlated with loss of petals within the buttercup family (Ranunculaceae). *Proc. Natl. Acad. Sci. U.S.A.* **110**, 5074–5079 (2013).
44. D. S. Skopelitis, A. H. Benkovics, A. Y. Husbands, M. C. P. Timmermans, Boundary formation through a direct threshold-based readout of mobile small RNA gradients. *Dev. Cell* **43**, 265–273.e6 (2017).
45. S. Yoshida, A. v. d. Schuren, M. van Dop, L. v. Galen, S. Saiga, M. Adibi, B. Moller, C. A. T. Hove, P. Marhavy, R. Smith, J. Friml, D. Weijers, A SOSEKI-based coordinate system interprets global polarity cues in *Arabidopsis*. *Nat. Plants.* **5**, 160–166 (2019).
46. C. M. Ha, G.-T. Kim, B. C. Kim, J. H. Jun, M. S. Soh, Y. Ueno, Y. Machida, H. Tsukaya, H. G. Nam, The *BLADE-ON-PETIOLE 1* gene controls leaf pattern formation through the modulation of meristematic activity in *Arabidopsis*. *Development* **130**, 161–172 (2003).
47. T. Toriba, H. Tokunage, T. Shiga, F. Nie, S. Naramoto, E. Honda, K. Tanaka, T. Taji, J.-I. Itoh, J. Kyozuka, *BLADE-ON-PETIOLE* genes temporally and developmentally regulate the sheath to blade ratio of rice leaves. *Nat. Commun.* **10**, 619 (2019).
48. T. Blein, A. Pulido, A. Vialette-Guiraud, K. Nikovics, H. Morin, A. Hay, I. E. Johansen, M. Tsiantis, P. Laufs, A conserved molecular framework for compound leaf development. *Science* **322**, 1835–1839 (2008).
49. D. Vlad, D. Kierzkowski, M. Rast, F. Vuolo, R. Ioio, C. Galinha, X. Gan, M. Hajheidari, A. Hay, R. Smith, P. Huijser, C. Bailey, M. Tsiantis, Leaf shape evolution through duplication, regulatory diversification, and loss of a homeobox gene. *Science* **343**, 780–783 (2014).
50. Y. Wang, S. Strauss, S. Liu, B. Pieper, R. Lymbouridou, A. Runions, M. Tsiantis, The cellular basis for synergy between *RCO* and *KNOX1* homeobox genes in leaf shape diversity. *Curr. Biol.* **32**, 3773–3784.e5 (2022).
51. K. Sarvepalli, M. Gupta, K. Challa, U. Nath, Molecular cartography of leaf development – role of transcription factors. *Curr. Opin. Plant Biol.* **47**, 22–31 (2019).
52. J. Kim, H. Kende, A transcriptional coactivator, AtGIF1, is involved in regulating leaf growth and morphology in *Arabidopsis*. *Proc. Natl. Acad. Sci. U.S.A.* **101**, 13374–13379 (2004).
53. Y. Ichihashi, K. Kawade, T. Usami, G. Horiguchi, T. Takahashi, H. Tsukaya, Key proliferative activity in the junction between the leaf blade and leaf petiole of Arabidopsis. *Plant Physiol.* **157**, 1151–1162 (2011).
54. W. Arthur, *Evolution: A Developmental Approach* (Wiley-Blackwell, 2011).
55. P. Prusinkiewicz, Y. Erasmus, B. Lane, L. Harder, E. Coen, Evolution and development of inflorescence architectures. *Science* **316**, 1452–1456 (2007).
56. D. Raup, Geometric analysis of shell coiling: General problems. *J. Paleo.* **40**, 1178–1190 (1966).
57. N. Hervieux, M. Dumond, A. Sapala, A.-L. Routier-Kierzkowska, D. Kierzkowski, A. Roeder, R. Smith, A. Boudaoud, O. Hamant, A mechanical feedback restricts sepal growth and shape in *Arabidopsis*. *Curr. Biol.* **26**, 1019–1028 (2016).
58. C. M. Herrera, X. Cerdá, M. B. García, J. Guitián, M. Medrano, P. J. Rey, A. M. Sánchez-Lafuente, Floral integration, phenotypic covariance structure and pollinator variation in bumblebee-pollinated *Helleborus foetidus*. *J. Evol. Biol.* **15**, 108–121 (2002).
59. J. Schindelin, I. Arganda-Carreras, E. Frise, V. Kaynig, M. Longair, T. Pietzsch, S. Preibisch, C. Rueden, S. Saalfeld, B. Schmid, J.-Y. Tinevez, D. White, V. Hartenstein, K. Eliceiri, P. Tomancak, A. Cardona, Fiji: An open-source platform for biological-image analysis. *Nat. Methods* **9**, 676–682 (2012).
60. X. Yu, X. Duan, R. Zhang, X. Fu, L. Ye, H. Kong, G. Xu, H. Shan, Prevalent exon-intron structural changes in the *APETALA1/FRUITFULL*, *SEPALLATA*, *AGAMOUS-LIKE6*, and *FLOWERING LOCUS C* MADS-box gene subfamilies provide new insights into their evolution. *Front. Plant Sci.* **7**, 598 (2016).
61. L.-T. Nguyen, H. A. Schmidt, A. von Haeseler, B. Q. Minh, IQ-TREE: A fast and effective stochastic algorithm for estimating maximum-likelihood phylogenies. *Mol. Biol. Evol.* **32**, 268–274 (2015).
62. S. Kalyaanamoorthy, B. Q. Minh, T. K. F. Wong, A. v. Haeseler, L. S. Jermiin, ModelFinder: Fast model selection for accurate phylogenetic estimates. *Nat. Methods* **14**, 587–589 (2017).
63. M. Javelle, M. C. P. Timmermans, *In situ* localization of small RNAs in plants by using LNA probes. *Nat. Protoc.* **7**, 533–541 (2012).
64. S. Teotia, D. Zhang, G. Tang, Knockdown of rice microRNA166 by short tandem target mimic (STTM). *Methods Mol. Biol.* **1654**, 337–349 (2017).

Acknowledgments: We would like to thank M. Rausher and all the laboratory members for helpful discussions. **Funding:** This work is funded by the Strategic Priority Research Program of the Chinese Academy of Sciences grant (XDB27010304; to H.K.), National Natural Science Foundation of China grant (31930008; to H.K.), Chinese Academy of Sciences grant (ZDBS-LY-SM022 and GJTD-2020-05; to H.K.), National Natural Science Foundation of China grant (32000177; to X.Yao), and National Postdoctoral Program for Innovative Talents (to J.C.). **Author contributions:** Conceptualization: J.C., X.Yao, X.L., and H.K. Methodology: J.C., X.Yao, and X.L. Investigation: J.C., X.Yao, X.L., L.Y., and X.D. Visualization: J.C., X.Yao, and X.L. Supervision: H.K. Writing—original draft: J.C. and H.K. Writing—review and editing: X.Yao, H.S., X.Yin, C.W., E.C., X.F., S.L., B.L., and H.K. **Competing interests:** The authors declare that they have no competing interests. **Data and materials availability:** All data needed to evaluate the conclusions in the paper are present in the paper and/or the Supplementary Materials.

Submitted 14 November 2022
Accepted 21 March 2023
Published 21 April 2023
10.1126/sciadv.adf8049